

Article

# Identifying Spatially Correlated Patterns between Surface Water and Frost Risk Using EO Data and Geospatial Indices

Panagiota Louka <sup>1,\*</sup>, Ioannis Papanikolaou <sup>1</sup>, George P. Petropoulos <sup>2,3</sup>,  
Kleomenis Kalogeropoulos <sup>2</sup> and Nikolaos Stathopoulos <sup>4</sup>

<sup>1</sup> Lab Mineralogy-Geology, Department of Natural Resources Development and Agricultural Engineering, Agricultural University of Athens, 11855 Athens, Greece; i.pap@aua.gr

<sup>2</sup> Department of Geography, Harokopio University of Athens, El. Venizelou St., 70, Kallithea, 17671 Athens, Greece; gpetropoulos@hua.gr (G.P.P.); kalogeropoulos@hua.gr (K.K.)

<sup>3</sup> School of Mineral Resources Engineering, Technical University of Crete, Kounoupidiana Campus, 73100 Crete, Greece

<sup>4</sup> School of Mining and Metallurgical Engineering, Sector of Geological Sciences, Laboratory of Technical Geology and Hydrogeology, National Technical University of Athens, 15780 Athens, Greece; nicksta81@gmail.com

\* Correspondence: p.louka@aua.gr; Tel.: +30-6944-140-612

Received: 13 January 2020; Accepted: 28 February 2020; Published: 4 March 2020



**Abstract:** Frost is one of the most significant hazards affecting various aspects of human lives including infrastructure, agriculture, economy and biodiversity. Water bodies are one of the key factors controlling temperature fluctuations and frost. This study introduces a contemporary method for identifying and spatially analyzing frost risk and also explores its spatial correlation with water bodies. The proposed technique is based on coupling freely distributed geospatial data with a time series of land surface temperature (LST) data from Moderate Resolution Imaging Spectroradiometer (MODIS) sensor. A region located in NW Greece, which annually suffers from very low temperatures and frost conditions and hosts important infrastructure and other human activities, was selected as a case study. In total, 5944 images were processed covering a 14-year long period. A frost frequency map of the study area was compiled along with two geospatial indices associated to distance from rivers/lakes (Hydro Distance Index—HDI) and from the seashore (Sea Distance Index—SDI). Their combined statistical and spatial correlation analysis indicated a protective buffer zone from frost at distances up to 20 km from sea and up to 5 km from lakes and rivers respectively, suggesting that the protective buffer zone depends on the water volume. Statistically, frost frequency was found to be positively correlated with both SDI ( $r_s = 0.527$ ) and HDI ( $r_s = 0.145$ ). Also, the effect of topography was examined in our analysis. Results showed that altitude and slope were moderately correlated to frost frequency; yet, the significance of the correlation was reported to be lower to SDI. Furthermore, the spatial autocorrelation analysis revealed a correspondence in the clustering of frost frequency maps with the HDI and SDI. Our findings demonstrate that water bodies are a major controlling factor for frost occurrence, by lowering frost frequency in water surrounding areas. Furthermore, it highlights the promising potential of our proposed methodology in quantifying frost effects, which can form a potentially useful tool assisting effective planning of protection measures and frost hazard mitigation in general.

**Keywords:** Greece; MODIS; spatial autocorrelation; water bodies; spatial data analysis; geospatial data

## 1. Introduction

Geoenvironmental hazards and extreme natural phenomena, such as, frost, desertification, forest fires and so forth, are affecting every year thousands of people globally. Water-related hazards are among the most severe and influential ones for human life. Climate change along with unsustainable human overexploitation of natural resources (qualitative and quantitative) has amplified the intensity and frequency of their occurrences as well as their impacts [1]. Consequently, research in fields such as flooding, rainfall, surface run-off decrease, and soil erosion is constantly evolving and enriched with contemporary techniques, tools and data [2–6]. Furthermore, the indirect impact and influence of surface water in natural processes that may lead to extreme phenomena such as extremely low temperatures and frost have also been extensively investigated [7–15].

The spatiotemporal distribution of extreme low temperatures and frost risk has been the subject of significant research during the recent decades. This is due to their severe consequences in infrastructure, agriculture, biodiversity and human society in general, which have constituted frost risk mapping as a major priority for environmental scientists and policy makers [16–20]. Major economic losses caused by freezing of horticultural crops are observed throughout the world annually [21–27]. Frost has been globally identified as a leading agricultural hazard, as it can occur in almost any location, outside the tropical zones [28]. About two thirds of the world's landmass is annually subjected to temperatures below the freezing point and about half of it suffers from temperatures below  $-20\text{ }^{\circ}\text{C}$  [29]. Apart from the economic losses, there are also significant secondary effects on local and regional communities, such as migration and unemployment [28].

Equally important are the severe impacts of frost on safe and timely transportation during winter months, even in countries with mild climate such as Greece. During periods with extreme weather conditions there is higher risk of car accidents caused by road slipperiness and in travelling delays due to lower commuting speed [30,31]. In more extreme weather, the road may be inaccessible even for emergency traffic such as ambulances, fire engines and police cars causing significant disturbances [32]. Taking into account of the severe consequences of frost, the ability of acquiring information on the distribution of frost events is of crucial importance and it is important to obtain information concerning not only when, but also where frost may occur in a region [33].

Nowadays, the rapid development in Earth Observation (EO) and Geographic Information Systems (GIS) has improved our ability to perform frost risk mapping and prediction [16,18,20]. Remote sensing data of higher spatial and temporal resolution are constantly released providing information concerning the spatiotemporal distribution of surface temperature [34]. Furthermore, different studies based on the implementation of GIS with EO data have focused on analyzing the effect of physiographic, topographic and human-induced factors in frost occurrence [35–37].

Various studies have manifested the importance of several factors of temperature fluctuation and frost risk [7–9,17,19,20,38–46]. These factors include geographical and geomorphological parameters, such as latitude [38], elevation [8,33,45,46], slope gradient and aspect [7,8,18,33,47,48], topographic curvature [45,49,50], soil moisture and distance from water bodies [7–15] and lastly, parameters connected to land use/cover, such as vegetation or human activity [41,44,45,51,52]. The presence of water surfaces and increased soil moisture have a protective role as far as frost risk is considered. In particular, water bodies with wide extent, such as lakes, large rivers and the sea, through their thermal inertia are connected to reduced frost risk levels, as they positively affect the temperature and movement of cold air masses and reduce the intensity of radiation frosts [7,8].

Soil moisture and atmospheric moisture near the ground level are important parameters of temperature fluctuation due to their effect on evapotranspiration [7]. In areas with high soil moisture, the irradiated energy first evaporates moisture and then heats the surfaces during the day. As a result, daytime temperatures in humid regions are significantly lower [53]. Similarly, during the night, increased soil moisture affects the variation of minimum temperature, limiting the prevalence of extreme low temperatures and the risk of frost on the land surface [54]. High levels of soil and

atmospheric moisture are mainly found in areas with high precipitation rates and proximal to large water bodies.

Building on previous studies [7–15], this study aims at investigating the correlation between frost frequency and distance from rivers, lakes and the sea, in an extended area of northwestern Greece, by processing and analyzing geospatial and satellite data via geostatistical techniques [55] and spatial indices. In the selected study area, the protective buffer of water bodies against frost was found to differentiate depending on the water volume, so longer protective distances were found to apply to the influence of the sea and shorter distances applied to the effect of lakes and rivers. Also, since frost occurrence is also influenced by other parameters and predominantly from landscape characteristics, our analysis has been expanded to cover these factors and compare their influence against water bodies.

## 2. Materials and Methods

### 2.1. Study Area

Our study area is situated in northwestern Greece and covers an area of 8661 km<sup>2</sup>, having a perimeter of 806 km (Figure 1). The area is characterized by extreme weather conditions during the winter months, where frost conditions often occur. The landscape can be described as a mosaic of extended flat shores in seaside regions and an alternation of valleys and mountainous areas with the highest altitude at 2204 m. In the eastern part, the study area is maritime with low elevations and mild slopes. In its central part the terrain is rough with mountain ranges trending mostly NNW-SSE following the alpine deformation field with steep slopes mainly facing ENE-WSW. The western part has a smoother relief with many rivers and streams flowing towards the sea.

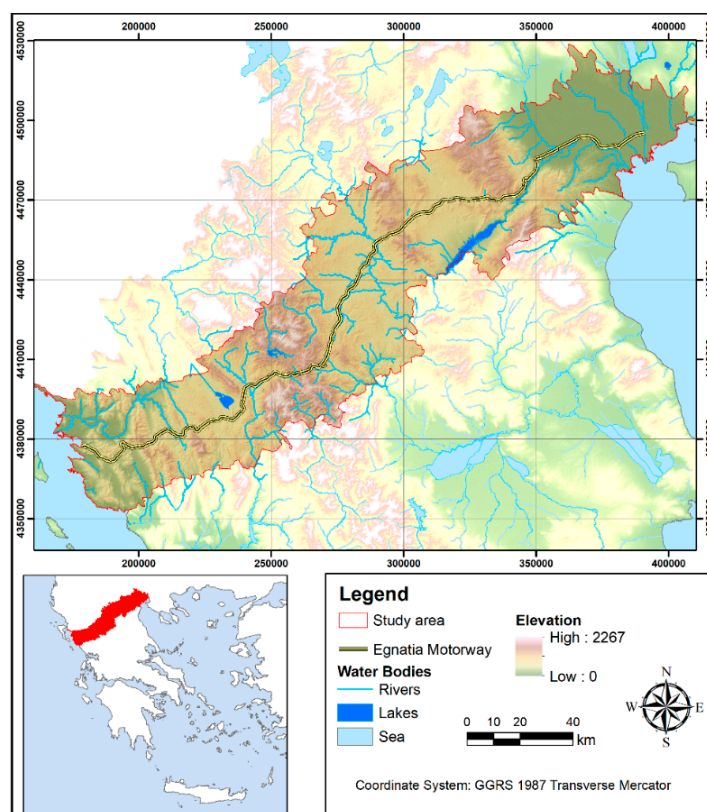


**Figure 1.** Geomorphological map of the study area, displaying the main water bodies.

This specific area was selected, as a suitable test site for applying the developed methodology, since it meets all the required criteria (dense and extended river network, lakes and proximity to the

sea, along with extremely frequent low temperatures and frost occurrence). In addition, it hosts major infrastructure, such as the Egnatia motorway (that is the predominant E-W trending transportation route in South Balkans), which often experiences traffic disruptions due to frost. Lastly, agricultural activities cover a major part of the studied area, which suffer from significant crop losses and financial damage due to frosting occurrence.

The study area was defined based on the road axis of Egnatia motorway, one of the most significant infrastructure works of Greece. A buffer zone of 15 km on each side of the western and central part of the motorway has been analyzed, covering a length of almost 310 km. This part of the Egnatia motorway has been found to be prone to weather extremes and terrain complexity. This is because it is situated in a mountainous region of northern Greece, where during winter and early spring, frost and snow conditions often occur. In general, the weather conditions along the motorway are diverse and sometimes extreme, applying significant stresses and costs on the operation and maintenance as the motorway crosses through rough landscape [56].

The main geological formations of the study area (flysch and Neogene marls) are impermeable increasing surface runoff, therefore a high-density hydrographic network is developed. The area's drainage network is extensive and includes parts of the catchments of Greece's three major river systems (Aliakmonas, Kalamas and Arachthos). Furthermore, the study area includes Pamvotida, the 9th largest lake of Greece covering an area of almost 20 km<sup>2</sup>, as well as the artificial lakes of Polyfitos (74 km<sup>2</sup> area) and Aaos (12 km<sup>2</sup> area).

## 2.2. Data

In our study a range of freely distributed geospatial datasets were combined, processed and analyzed, which are summarized in Table 1 below.

**Table 1.** Data information.

Data	Information Derived
Geographic Information Systems (GIS) data	Hydrographic network, Lakes Coastal water surfaces
Moderate Resolution Imaging Spectroradiometer (MODIS) data	Land Surface Temperature (LST)
Advanced Spaceborne Thermal Emission and Reflection Radiometer (ASTER) Global Digital Elevation Model (GDEM)	Digital Elevation Model

GIS data were obtained from the national open database of Greece. Three different vector layers were acquired concerning the hydrographic network, lakes and coastal water surfaces.

Information on the spatiotemporal variability of Land Surface Temperature (LST) was obtained using MYD11A1 images retrieved from the Data Pool, courtesy of NASA EOSDIS Land Processes Distributed Active Archive Center (LPDAAC), USGS/Earth Resources Observation and Science (EROS) Center, Sioux Falls, SD, United States. The product MYD11A was selected from Aqua satellite which provides information on night-time LST with a spatial resolution of 1 km on a daily basis. These are Level 3 (L3) products in tiles of 1113 km<sup>2</sup> and their estimated accuracy is 1 °K in land and under clear sky conditions [57]. The study area is distributed in two MODIS tiles—column 19 and row 4 and 5. In total, a time series was created by processing 5944 images, which correspond to the period from the 1 October to the 30 April of the years 2003 to 2016.

In addition, information on topography was obtained from the ASTER (Advanced Spaceborne Thermal Emission and Reflection Radiometer) global digital Elevation Model V002 data, also available from the online Data Pool, courtesy of the NASA Land Processes Distributed Active Archive Center (LP DAAC), USGS/Earth Resources Observation and Science (EROS) Center, Sioux Falls, South Dakota, United States. The dataset comprised of the granules N40E21-22, has a spatial resolution of 30 m and a mean accuracy of 12.41–13.6 m for the area of Greece [58,59].

The software platforms used for the processing and analysis of the above data included ArcGIS 10.4 maintained by the Environmental Systems Research Institute (Esri) in Redlands, CA, United States, ENVI 5.1 (Environment for Visualizing Images) developed by Harris Geospatial Solutions (Broomfield, CO, United States), XLSTAT by Addinsoft (New York, NY, United States) and GeoDA developed by the Spatial Analysis Laboratory of the University of Illinois at Urbana-Champaign under the direction of Dr Anselin [60].

### 2.3. Methodology

#### 2.3.1. Overview

An overview of our proposed methodology is illustrated in Figure 2.

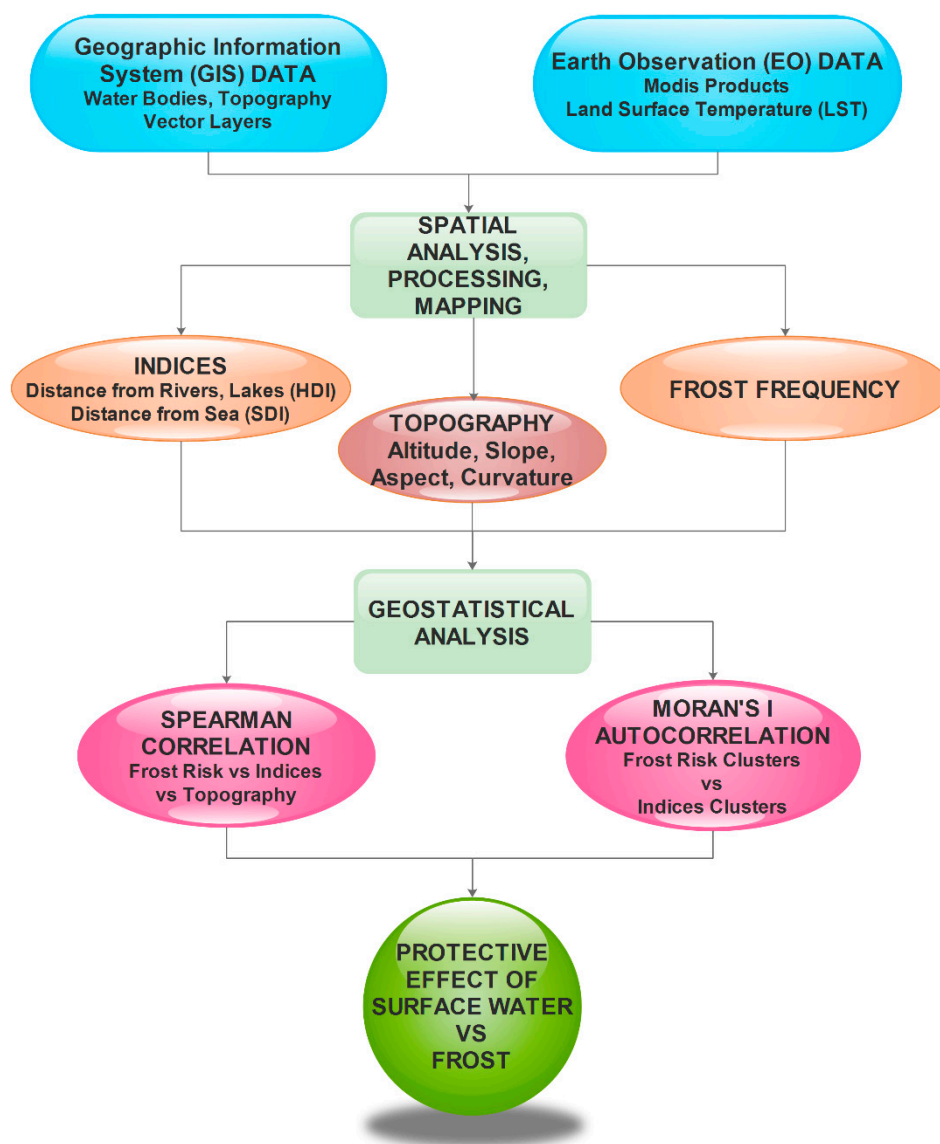


Figure 2. Flowchart of the methodology.

#### 2.3.2. Spatial Analysis of Water Bodies and Development of Indices

The first step involves the analysis of the inland water bodies (hydrographic network and lakes) and the development of HDI (Hydro Distance Index) and SDI (Sea Distance Index), which represent the spatial distribution and distance from rivers, lakes and the sea respectively. For these processes

two raster layers were created, with the same spatial resolution of MODIS LST images ( $0.926 \text{ km}^2$ ), so that consistency would be maintained for further data analysis.

The development of the HDI index which is based on the relative distance from lakes and rivers was accomplished by the following procedure. Firstly, the initial data (vector layers), concerning spatial information on the hydrographic network and lake distribution, were clipped according to the limits of the study area. Subsequently, a single vector layer was created by the union of the two initial layers after the lakes' layer was converted from polygon to polyline. Then the Euclidean distance from rivers and lakes was calculated and the corresponding raster file was created. Finally, a logarithmic transformation was performed using the natural logarithmic formula and the HDI was extracted.

$$\text{HDI} = \ln(\text{Euclidean Distance from Rivers/Lakes}) \quad (1)$$

Following the same procedure, the SDI was obtained (i.e., by the logarithmic transformation of the raster file containing the estimation of the Euclidean distance from sea).

$$\text{SDI} = \ln(\text{Euclidean Distance from Sea}) \quad (2)$$

The logarithmic transformation of distance was selected as more representative of the protective effect of water bodies against frost risk, as the intensity of the effect of water surfaces on temperature fluctuations decreases with distance very abruptly and not linearly [29,33,36].

### 2.3.3. Frost Frequency Analysis

Frost frequency analysis in the study area was performed by processing the MODIS LST time series data (from the MYD11A1 product), covering a 14-year period from 1st of October to 30th of April of the years 2003–2016. The frost frequency map of the study area was compiled following the methodology described in a previous study by [61]. The processing of the images included the identification of areas where land surface temperature was below  $0 \text{ }^\circ\text{C}$ . The latter indicated frost conditions and the identification of areas where temperature information was recorded and distinguished from the no data areas (due to cloud cover or other cause). The next step involved the stacking and summing up of the results of the two processes in two corresponding composite images.

Finally, the frost frequency map was compiled, based on the two composite images, which presents the frost frequency in relation to frequency of temperature detection by MODIS instrument. The values of the frost frequency map ranged between 0 and 1 and corresponded to the times frost had been detected per the times temperature information was available for each cell of the frost frequency map. So, '0' values corresponded to no frost detected in the images where temperature information was available and '1' values were assigned to cells where frost was recorded in all the images in which temperature information was available.

### 2.3.4. Topography Analysis

Frost occurrence is also influenced from the landscape characteristics. Therefore, the influence of topography has also been taken into consideration in our study and its relationship with the frost frequency map was investigated as well. In particular, the altitude, slope, aspect and curvature (Figure 3) were analyzed and their correlation to frost frequency and the two indices (HDI, SDI) has been evaluated.

In the aspect maps, a reclassification was required so as to assess the influence of the slope orientation in temperature variation. The initial aspect values were grouped in 3 categories depending on the amount of incoming solar radiation for each type of orientation [18,33,36] and their values were reclassified accordingly. So, Northfacing slopes receive the lowest amount of solar radiation and the value '1' was assigned to them. Southfaced slopes were assigned the value of '3' as incoming insolation is the highest in south facing areas. Lastly, western and eastern slopes were assigned the value of '2'.

No such transformations were necessary for the altitude, curvature and slope parameters.

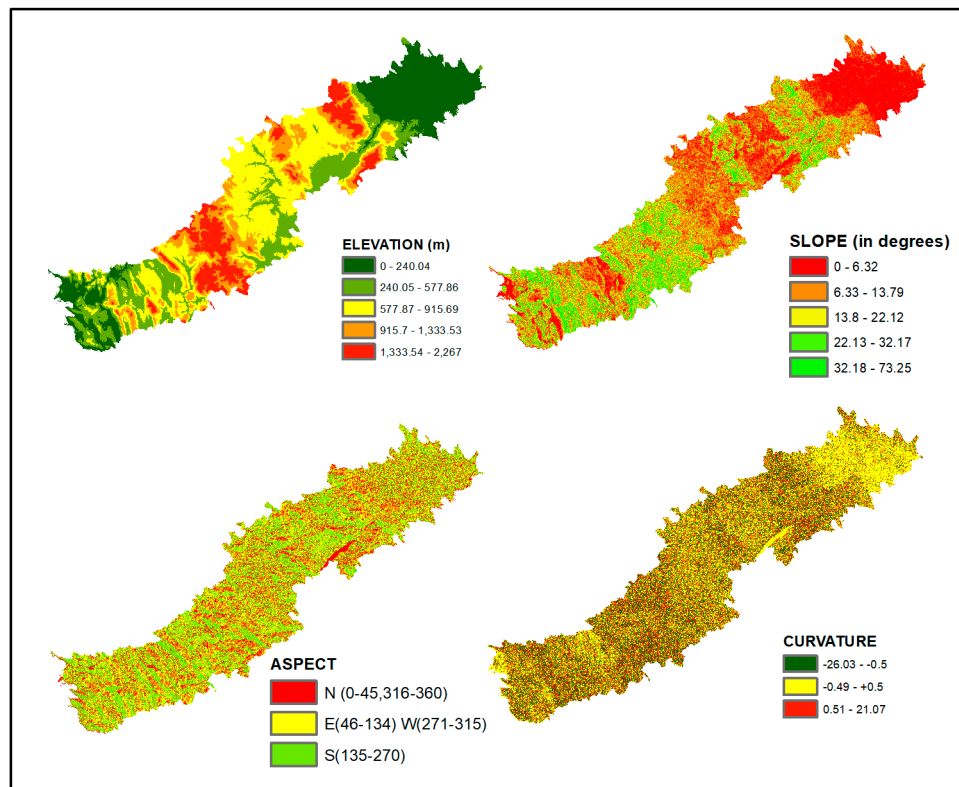


**Figure 3.** Spatial distribution of the following topography factors—Elevation, Slope, Aspect and Curvature.

### 2.3.5. Statistical Analysis

To assess the correlation between frost frequency, HDI, SDI and the landscape characteristics of the study area, the following procedure was implemented. Firstly, a vector point layer was created from the cell centroids of the frost frequency raster layer. Next, the cell values of the centroids of the layers of frost frequency, HDI, SDI and the topography factors of altitude, slope, curvature and slope aspect were extracted. An attribute table was created in ArcGIS, which consisted of approximately 13,000 point values. The table was extracted in Excel and was further processed with Excel's statistical extension, XLSTAT, in order to estimate the correlation among the raster layer values of the HDI, SDI and the frost frequency using Spearman's statistical index.

### 2.3.6. Moran's I Autocorrelation Analysis

The final step of the process concerned the analysis of the spatial distribution and the detection of spatial autocorrelation among frost frequency, HDI and SDI. This step is fundamental in identifying the spatial patterns and the distribution of the studied variables. Spatial autocorrelation analysis can assist in the documentation of the spatiotemporal variation and the understanding of the factors that have a crucial effect in phenomena linked to weather conditions [62].

The analysis was performed after following some key stages. Firstly, the point layer containing the centroid values of frost frequency, HDI and SDI was processed so as to estimate the spatial autocorrelation of all the layers by the local Moran's I statistical test (Local Indicators of Spatial Association—LISA) [63]. After several trials, the K6-nearest neighbor matrix was selected as the most representative and suitable for highlighting spatial patterns in the best possible way and identifying optimum clustering of the data based on low and high statistically important values. The result of this procedure was a map showing clusters of significant high and low values and a scatter plot indicating the Moran's I values for each variable (frost frequency, HDI and SDI).

### 3. Results

#### 3.1. Spatial Distribution of HDI and SDI

The spatial distribution of HDI and SDI in the study area is presented in Figures 4 and 5 correspondingly. They provide information on the relative distance of each point of the study area from rivers and lakes (Figure 4) and the sea (Figure 5). These maps present the study area categorized in five classes depending on the values of the indices. The maps categorization is implemented using the Natural Jenks method. It is a data classification method that is based on the natural grouping inherent in the data and maximizes the differences between classes [64]. However, the processing and evaluation of the results was executed on the original indices values and not on the classes presented in the maps.

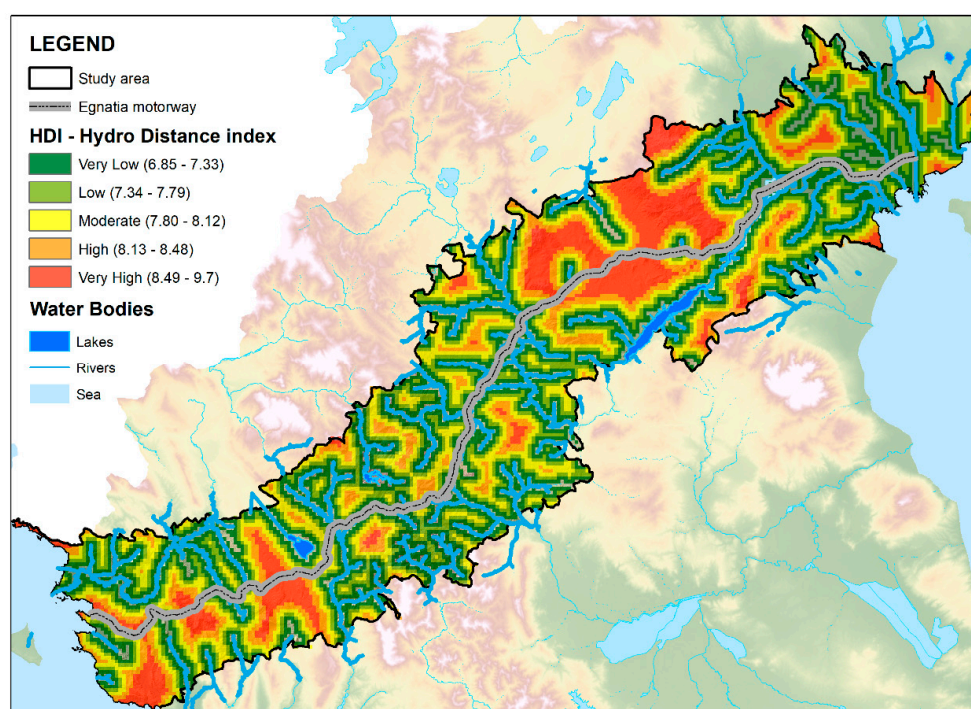


Figure 4. Spatial distribution of the HDI (Hydro Distance Index).

In the two maps (Figures 4 and 5), we can see red colored areas where the values of the indices are higher, which correspond to higher frost risk areas, as they lie outside of the protective buffer zones of water bodies. On the contrary, green colored areas, where the indices have lower values, are contained in areas more protected from frost risk due to the effect of water bodies. By observing these maps, the lateral proximity of the study area to the sea is evident in contrast to the diffused and varied dispersion of water bodies (lakes-rivers).

#### 3.2. Spatial Distribution of Frost Frequency

The frost frequency map of the study area, based on MODIS surface temperature data is illustrated in Figure 6. The map highlights areas where frost frequency is high (red colored), in contrast to other areas (yellow and green colored). Significant variability in frost frequency is observed across the study area, even over short distances. The high variability reflects the rough landscape as a result of the intense Alpine orogenic processes that influenced all the geomorphic parameters (such as slope, slope aspect, etc.) that affect frost distribution.

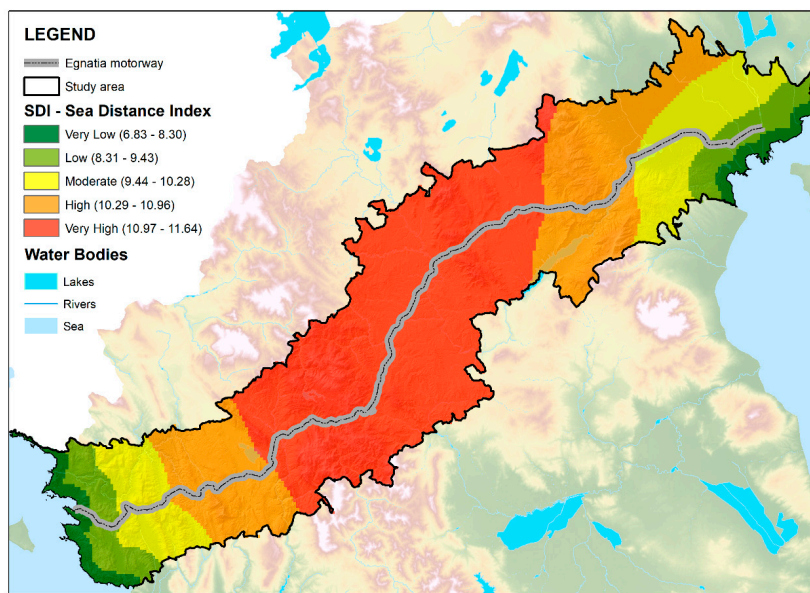


Figure 5. Spatial distribution of the SDI (Sea Distance Index).

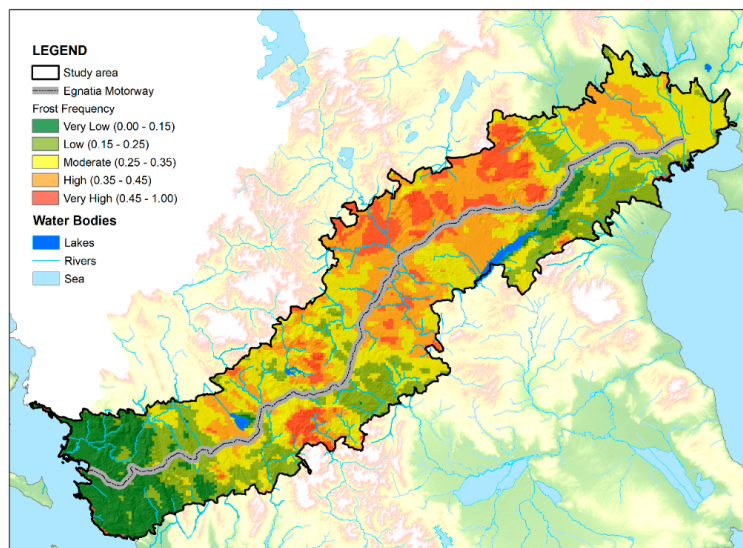


Figure 6. Frost frequency map of the study area showing the Egnatia motorway and the surrounding water bodies.

By examining the frost frequency map from west to east, we can firstly see the very low and low frost frequency zones in the western part which extend over an area up to 20 km from the sea. As shown in the geomorphological map (Figure 1), this region is characterized by intense relief with an altitude up to 1450 m and is crossed by the branches of two major rivers.

Then further to the east, a moderate to high frost frequency zone is traced. This is the most rough and high altitude terrain along the study area, reaching up to 2000 m elevation. Two lakes are observed within this part, the western is Pamvotida (500 m altitude) and the eastern is the artificial lake that is filled by the sources of the AooS river (1300 m altitude). The influence of those two lakes against frost frequency seems to extend up to distances of 5 km.

Eastwards, there is an area of moderate altitude, surrounded by two mountain ranges, according to the geomorphological map of Figure 1. Several major rivers cross this region and although altitude does not differentiate in this region, frost frequency varies from low to high levels.

The next part of the study area is very mountainous in the north without any major rivers and very high to high frost frequency was recorded. On the contrary, its south part includes branches of a major river as well as the artificial lake of Polyfitos. Moderate to very low frost frequency has been recorded in this part, which can be attributed to the combined effect of the lake, the river that supply the lake, as well on the surrounding topography.

The eastern end of the study area is of great interest, as it is a low land region, a valley which is crossed by three major rivers that flow into the sea where agricultural activities dominate. Contrary to what might be expected, moderate to high frost frequency was recorded in the area and only small regions of low frost frequency are observed in the coastal zone, reaching to distances up to 5 km from the sea.

Figure 6 displays the distribution of frost occurrence along the Egnatia motorway and some key observations can be extracted. About half of the road length lies in areas of moderate to high frost risk. Especially the central part of the motorway crosses areas of high frost frequency, as they are exposed to low temperatures during the winter months. The western part of the motorway is in an area of very low—low frost risk, which can be attributed mainly to the short distance from the sea. Also, the north-central part of the motorway is characterized by low to moderate frost risk. In this area, the drainage network is dense and in particular some rivers cross the area at short distances from the motorway. Lastly, the eastern tip of the motorway is characterized by low frost occurrence, which can be attributed to the combined influence of the sea, lakes and rivers that prevent frost phenomena in the area.

### 3.3. Statistical Analysis

The recorded frost frequency levels as well as the spatial distribution of HDI and SDI were analyzed in order to quantify and evaluate the correlation between the indices and frost frequency.

In addition, the effect of topography on the variation of frost frequency, HDI and SDI was explored, by incorporating the factors of altitude, slope, curvature and slope aspect. Table 2 displays the results of the correlation analysis of frost frequency in relation to the HDI, SDI and the topographic parameters, using the Spearman's correlation coefficient ( $r_s$ ). The  $r_s$  values that indicate moderate ( $r_s \geq 0.3$ ) and strong ( $r_s \geq 0.5$ ) correlation are marked in bold.

**Table 2.** Spearman's statistical correlation analysis ( $r_s$ ) among frost frequency, SDI, HDI and topography.

Variables	Frost Frequency	SDI	HDI	Altitude	Slope	Aspect	Curvature
Frost Frequency		<b>0.527</b>	0.145	<b>0.306</b>	−0.193	−0.002	−0.02
SDI			−0.052	<b>0.589</b>	0.147	0.010	−0.018
HDI				0.260	−0.061	0.009	−0.023

Note: HDI, Hydro Distance Index; SDI, Sea Distance Index.

Table 2 shows that there is a strong positive correlation between frost frequency and distance from the sea, as the Spearman's correlation coefficient is 0.527, indicating that as the distance from sea increases, frost frequency is higher. The correlation between frost frequency and distance from water bodies is still a positive one, but has a relatively low value ( $r_s = 0.145$ ), indicating a rather weak correlation. The conclusion that can be drawn is that even though there is a clear tendency for increased frost occurrence in areas far from lakes and rivers this is not statistically strong for our study area. This is probably because other factors are also superimposed (e.g., altitude, aspect) on the frost occurrence. Concerning the topography effect on frost frequency distribution, it can be observed that altitude is the dominating factor in our analysis, as the Spearman's correlation coefficient is 0.306, showing a moderate correlation; however, it is lower to the correlation of frost risk with SDI. Also, slope has a weak negative correlation with frost frequency, indicating that there is a reverse correlation between frost and slope steepness so that frost frequency is higher in relatively flat areas. This is consistent to

previous findings [18,33,36]. Lastly, curvature and slope aspect do not seem to be correlated to frost frequency, which can be attributed to the raw spatial resolution of MODIS images from which the frost frequency was derived.

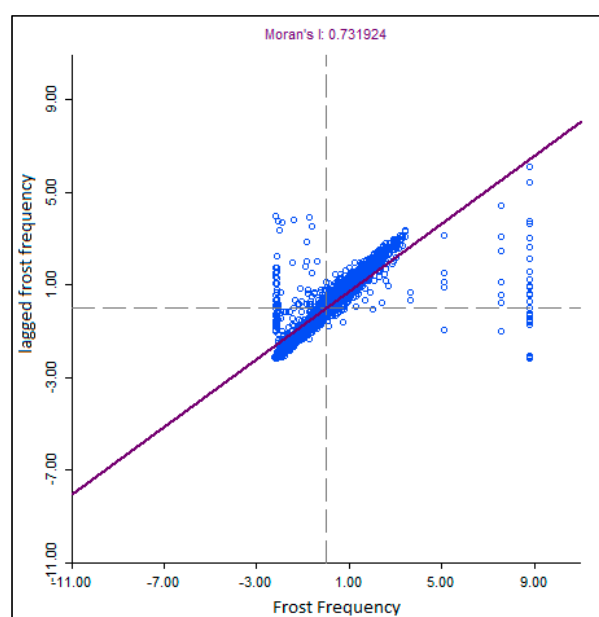
As for the SDI distribution, it is also strongly correlated to the altitude, which was expected as coastal areas generally are by definition at or near sea level. However, there is not a perfect positive correlation, showing that the variation of SDI can be only partly linked to altitude fluctuations. The other topographic factors have a weak correlation with the SDI. It is important to note that, according to our results, the SDI and HDI are not correlated, as the Spearman's correlation coefficient is  $-0.052$ , which indicates that the two variables are independent to each other.

Lastly, the HDI correlation to topography is basically linked to altitude as there is a moderate positive correlation ( $r_s = 0.260$ ), indicating that since water flows with gravity, water bodies tend to be concentrated in lower altitudes. HDI does not seem to correlate with slope, curvature and aspect, as the Spearman's correlation coefficient values are very low, close to zero.

### 3.4. Spatial Autocorrelation

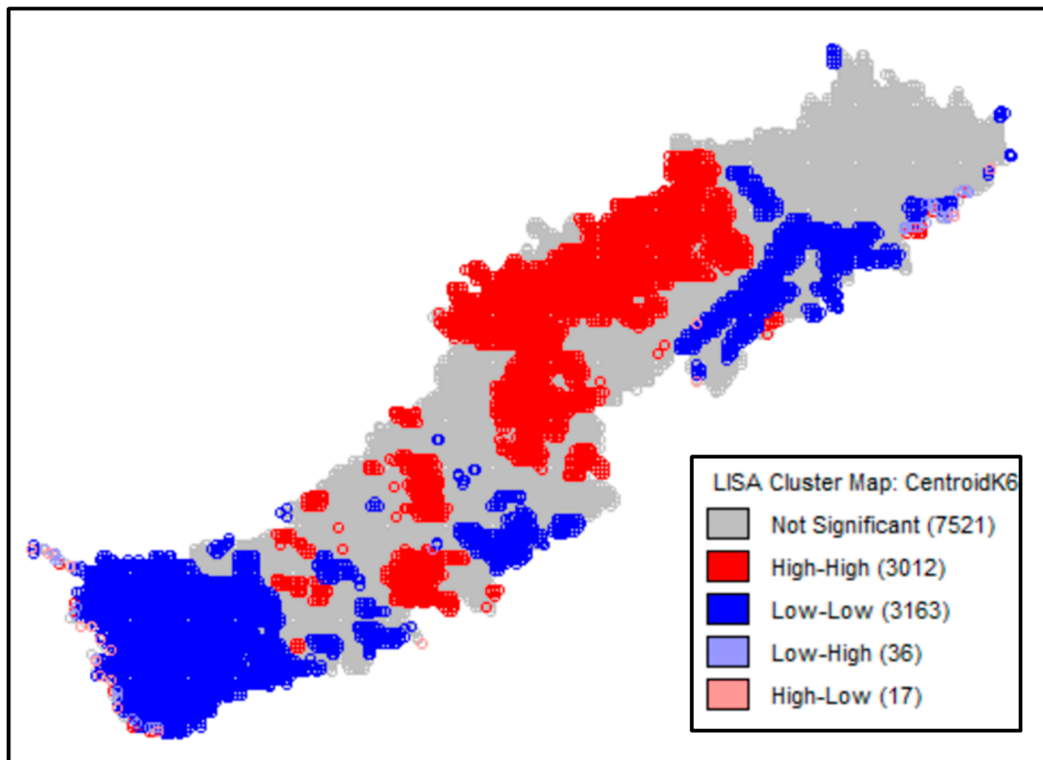
The spatial patterns of frost frequency with the HDI and SDI distribution in the study area were further investigated. The degree of spatial autocorrelation of the indices and frost frequency and the identification of areas with significantly lower or higher values was attempted based on the local Moran's I statistical test, using the K6-nearest neighbor matrix. The existence of spatial clusters was investigated, which refers to areas where the values of a variable are more similar to its surrounding areas compared to a spatial randomness case study.

The maps of spatial patterns included classification of the study area based on the statistically significant values of the local Moran's I index into five classes, with a statistical significance level of 0.005. Figures 7–9 show the produced LISA cluster maps, which classify the study area by type of spatial autocorrelation, as well as the scatterplots of the clustering of frost frequency, the SDI and HDI. The dark red locations represent spatial clusters of high values surrounded by high values, forming a high-high region. Respectively, the dark blue locations indicate spatial clusters with low values surrounded by low values, forming a low-low region. The spatial outliers are regions with high values surrounded by low value regions or the opposite and are marked with light red or light blue and are called high-low and low-high regions respectively.



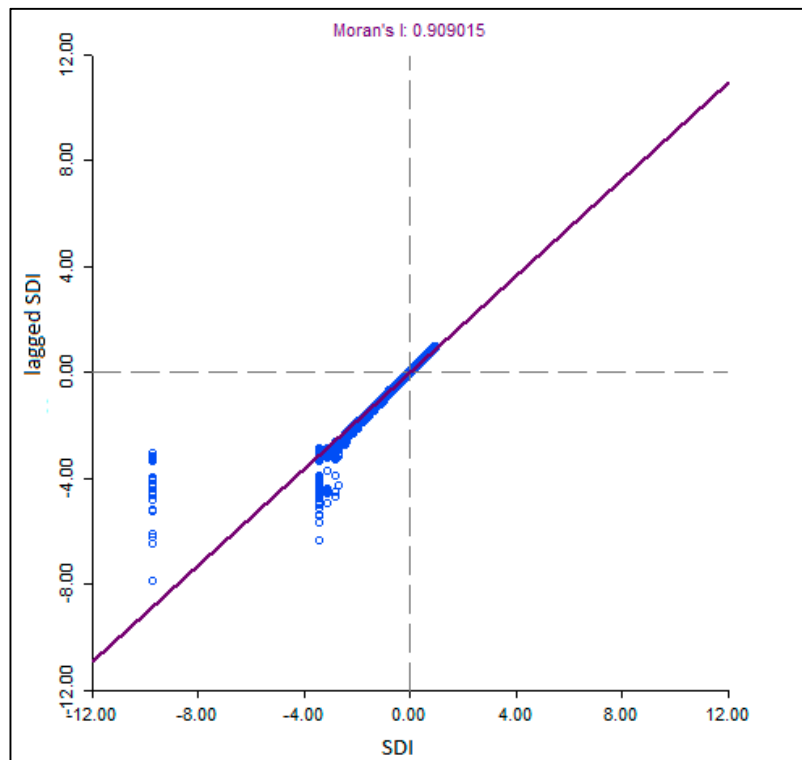
(a)

Figure 7. Cont.



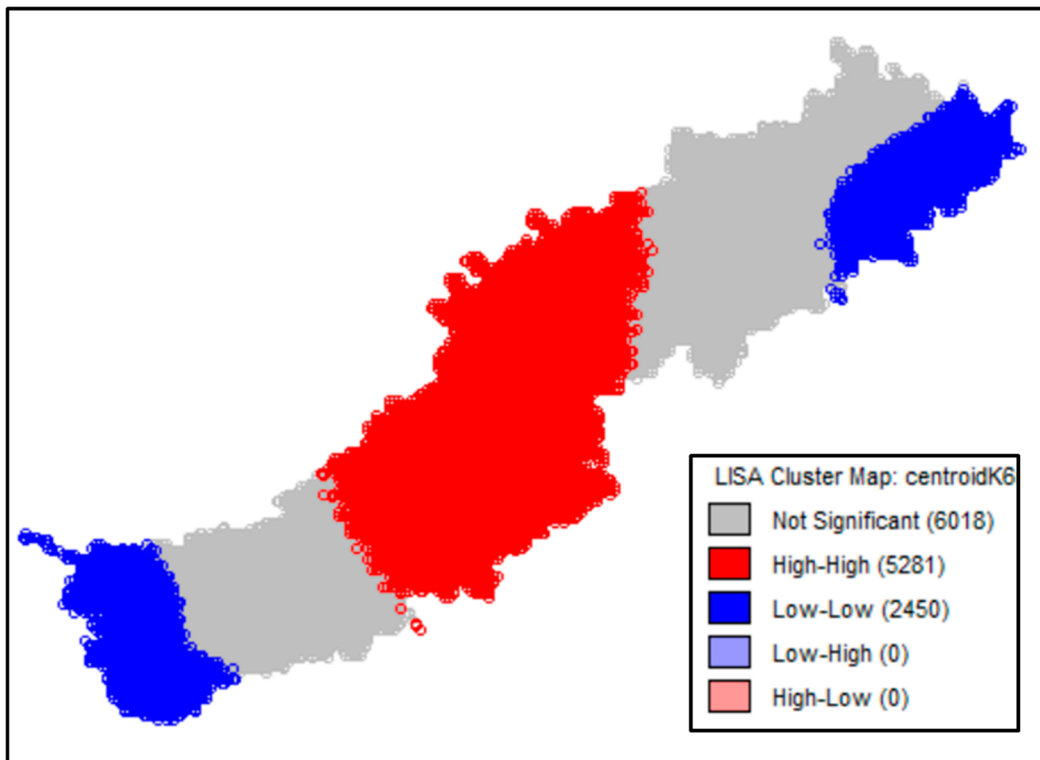
(b)

Figure 7. Autocorrelation map of frost frequency—(a) scatter plot and (b) cluster map.



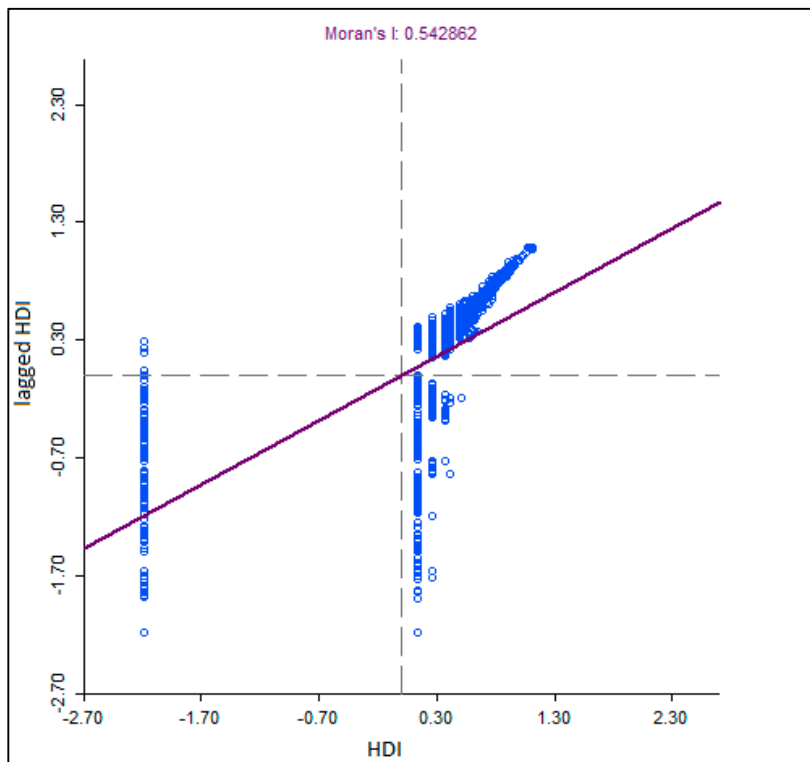
(a)

Figure 8. Cont.



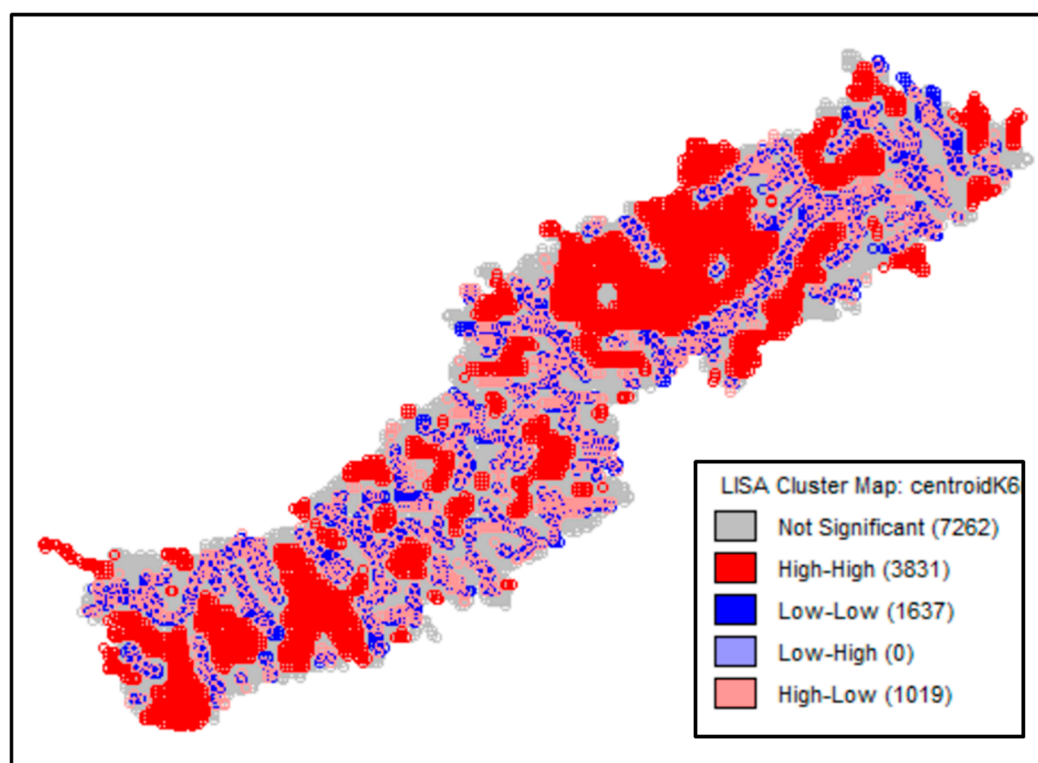
(b)

Figure 8. Autocorrelation map of the SDI (Sea Distance Index)—(a) scatter plot and (b) cluster map.



(a)

Figure 9. Cont.



(b)

**Figure 9.** Autocorrelation map of the HDI (Hydro Distance Index)—(a) scatter plot and (b) cluster map.

In Figure 7 frost frequency is presented based on the statistically significant values of the local Moran's I index into five classes. The existence of areas with statistically high frost frequency values is obvious in the central and north-central sections of the study area. In major parts of these regions, clusters of high SDI and HDI values have been identified (Figures 8 and 9), indicating that high frost frequency clusters could be linked to limited proximity to sea and water bodies. An extended cluster of significantly low frost frequency is observed in the western end of the study area. The latter can be linked to a similar but not so extended low SDI cluster near the coastline and to a smaller and scattered low HDI cluster. This indicates that low levels of frost risk in this area could be attributed to a great extent to the combined effect of sea and water bodies. Similar assumptions can be made concerning the low frost frequency cluster in the eastern part of the study area. According to the scatterplot of Figure 7, the Moran's I value is positive (Moran's I = 0.73), indicating that there is an overall pattern of clustering of frost frequency values. The above results suggest a strong positive spatial autocorrelation that is statistically significant.

The map presenting the classification of the study area in 5 classes depending on the values of the SDI is presented in Figure 8. Significantly low values are clustered in the western and eastern parts of the study area, extending to a zone of about 10 km from the coastline. The western low cluster shows a significant correspondence to the low cluster of the frost frequency map, which confirms the low levels of frost frequency of the area. The eastern low cluster has a similarity to the low clusters of frost frequency only towards its south part, indicating that other frost risk factors dominate in the rest of the area. An extended cluster of high SDI values is noticed in the central part of the study area. This region is not proximal to the sea and, in a major part of its extent, clusters of high frost frequency have been identified. In the scatterplot of Figure 8, Moran's I value is positive and quite close to 1 (Moran's I = 0.91), indicating that the SDI values are highly clustered.

Lastly, the study area map which refers to the values of the HDI and is classified in 5 classes is presented in Figure 9. The low clusters of HDI, which can be linked to the protective effect of water

bodies against frost, seem intensely concentrated around the riverbeds and the lakes and they are surrounded by outliers (high-low areas). From the HDI cluster map, it can be derived that statistically significant low values of the HDI, extend to short distances from water bodies, reaching up to 5 km from riverbeds and lakeshores. On the contrary, high clusters which refer to areas where the HDI values are significantly higher, cover larger areas, over which there is no protective effect of water bodies against frost as the hydrographic density is low. The strong positive correlation of the HDI clusters, which is statistically significant as Moran's I value is above 0.5, is presented in the scatterplot of Figure 9 (Moran's I value is 0.54).

In order to enhance the evaluation of the auto correlation analysis, Figure 10 has been produced showing the frost frequency in relation to the water bodies and the sea. It displays frost frequency spatial distribution, the high and low value clusters of frost frequency as well as the water bodies of the study area and the sea. The analysis of this map highlights the existence of statistically significant low frost frequency in the western part of the study area. This zone of low frost frequency extends up to 20 km from the sea and is crossed by two major rivers that flow into the sea, Kalamas (symbolized as R1 in Figure 10) and Acherontas (R2). Another region of low frost frequency is located in the eastern part, in distances up to 5 km from the artificial lake of Polyfitos (L3) and the riverbanks of the Aliakmon river (R4). Also, in the south-central part, there is a low frost frequency zone extending up to distances of 5 km from river channels that form part of the Pineios drainage network (R3). Two low frost frequency clusters of smaller extend are located next to the lakes of Pamvotida (L1) and Aaos (L2) reaching up to 3.5 km from the shore lakes. Lastly, a major high frost frequency cluster is traced in the central part of the study area. This high cluster is in a high-altitude area (600–2000 m) promoting frost occurrence. Even though towards its western part it is crossed by a rather dense drainage network, frost occurrence is still high because these catchments are small, drain small water quantities, thus having a lower impact on frost occurrence.

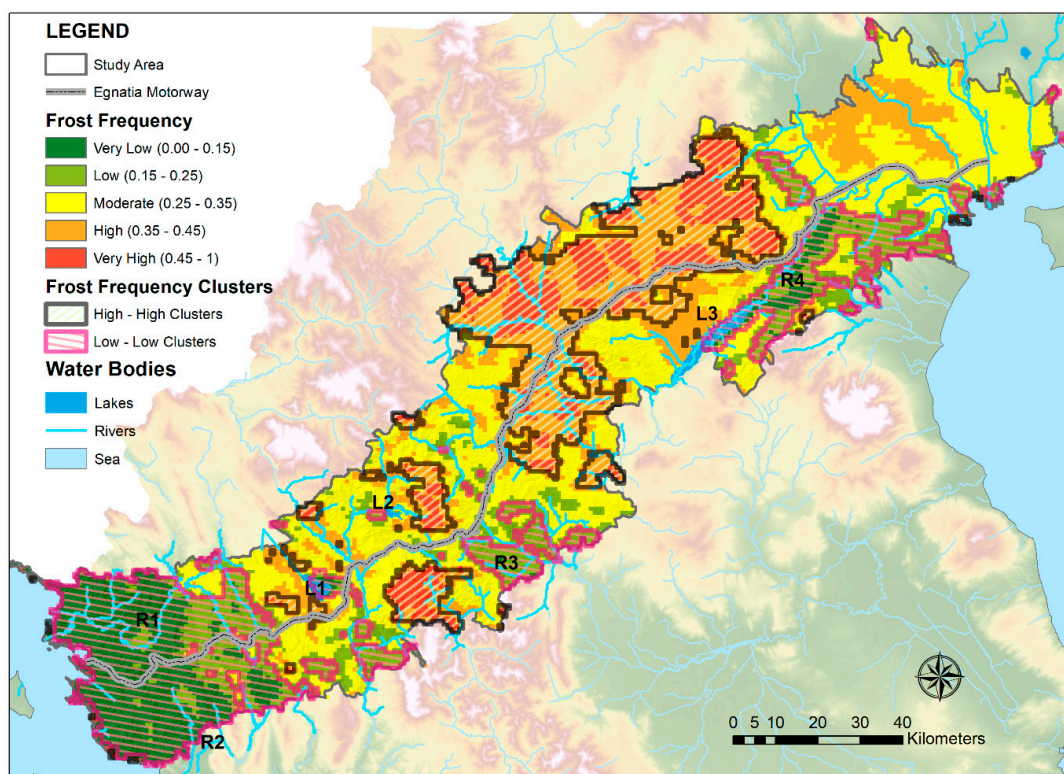


**Figure 10.** Frost frequency map, displaying the high and low frost frequency clusters and the drainage network of the study area.

Figure 10 provides also a frost hazard assessment along the Egnatia motorway. From west to east, the first 60 km of the motorway cover a low frost frequency area, partly attributed to the protective effect of the sea and the surrounding rivers. The next 90 km of the motorway crosses an area of moderate frost frequency levels, which includes a low frost frequency zone of almost 3 km, close to the lake Pamvotida and then for the next 60 km again the motorway crosses an area mainly of moderate frost risk levels. Then, there is the part of the Egnatia motorway which is most prone to frost (with a length of almost 85 km) where a high frost frequency cluster is observed. During winter, high levels of preparedness are required along this part of the motorway for timely mitigation measures against frost. Lastly, the remaining 70 km of the motorway are classified as moderate frost risk zone.

#### 4. Discussion

The present study analyzed the protective effect of surface water bodies (rivers, lakes, sea) against frost risk in an area of northwestern Greece. The hydrographic network (including lakes) and water bodies in general have been identified as one of the most important factors in differentiating surface temperature and reducing frost frequency [29,33,36,59]. The mechanisms involved in the protective effect of water against frost are associated to the thermal inertia of water bodies of wide extend and to the evapotranspiration of soil moisture, which prevents extreme temperature phenomena, such as frost [7,8,53].

Research on the influence of rivers on temperature variation has been carried out by Fridley [7]. In particular, the distance from rivers was used as an index for predicting surface temperature variation and a steady trend of higher relative temperatures was found in areas close to rivers. More specifically, areas within distance of 1 km from rivers, were found to be warmer with differences up to 2 °C [7]. Furthermore, the effect of a lake (Salt Lake Uyuni, 800 km<sup>2</sup>) on surface soil temperature was studied by Pouteau et al. in an area of Bolivia [36]. The lake was found to pose a substantial influence on the local surface temperatures up to a distance of 10 km and as a result, it prevents frost phenomena. Similar findings have been confirmed by the current study, even though they offer mostly a qualitative assessment rather than a quantitative one.

A frost frequency map was generated by EO data, obtained by MODIS sensor with spatial analysis of 1 km<sup>2</sup>. According to this map, the effect of sea and lakes—rivers on the risk of frost fluctuations appear to extend to a zone of 20 km and 5 km respectively. These results are in agreement with other similar studies from different settings [29,33,36,59].

According to the frost frequency map, topography seemed to pose an influence on frost occurrence, which is consistent to previous studies [7,8,33]. However, a significant part of frost variation was not linked to the landscape features of the study area. For example, in the western region of our study area, low frost frequency was recorded although its undulating terrain and altitudes up to 1450 m. Also, in the lowland valley located in the eastern end of our study area, moderate to high frost frequency was found. Only in the region close to the coast and towards the artificial lake, there were lower frost frequency levels.

Our research included also the statistical correlation analysis between frost frequency and water bodies. Frost frequency and distance from the sea displayed a very strong positive correlation implying that the risk of frost increases with distance from the sea. In addition, a similar but lower correlation existed between frost frequency and the distance from lakes and rivers. However, this correlation needs further study due to the shorter buffer zones involved in lakes and rivers; therefore a higher spatial resolution is required. It is expected that the water volume influences the extend of the buffer zone and a higher spatial resolution can clearly resolve and quantify these effects in the surrounding area of rivers and lakes.

Furthermore, the statistical correlation of frost frequency, HDI, SDI and the topographic parameters were analyzed, in order to assess also the effect of topography in our results. Altitude and slope displayed moderate levels of correlation to frost frequency but lower compared to the correlation

between SDI and frost frequency. This finding is also in accordance to previous studies which have found that the influence of the topographic factors varies according to the scale of study [7,8].

Frost risk spatial variability in relation to surface water bodies was further investigated by analyzing the spatial autocorrelation patterns of frost frequency and the HDI and SDI distribution. The cluster maps of frost frequency and SDI displayed a similar spatial pattern across several regions of the study area. Clusters of high SDI values are observed in the central parts of the study area which are more prone to low temperatures and frost risk in the winter months. On the contrary, low SDI clusters are observed in the western and eastern edges of the study area where frost risk occurrence is lower. In addition, the frost frequency and the HDI map seem to follow a similar pattern in the eastern central regions of the study area. Clusters of high frost risk are observed in parts of clusters of high HDI values. These areas are more susceptible to frost risk and are characterized by low density of surface water bodies.

Lastly, the proposed methodology was applied on a major infrastructure work, the Egnatia motorway, showing that a more accurate zonation in relation to frost risk can be accomplished through this application. An enhanced ability to predict frost risk along the motorway can be achieved which can lead to planning of more effective mitigation measures.

To sum up, according to the results of this study, the effect of sea on the temperature fluctuations and frost frequency is obvious and appears to extend at a zone up to 20 km. However, our results suggested that the effect of lakes and rivers is less intense and more variable, as it extends at distances up to 5 km, which is in agreement with findings of other studies [7,8]. Also, it is worth noting that the effect of lakes and rivers generally depends on their relative size and water volume and occasionally may be overprinted on a case by case basis by other factors, such as altitude, slope and slope orientation (aspect). Our analysis regarding the topographic parameters and the frost frequency showed that the altitude and the slope exert the main influence at least for such square km scales provided by MODIS data. It is expected that the other topographic parameters such as aspect and curvature can be identified in studies of higher spatial resolution [7,8] since their characteristics change significantly on the sub-km scaling.

The application of the methodology presented in this work can have a significant contribution to research related to the risk posed by extreme low temperatures and to the targeted design of mitigation measures. It must be underlined that the methodology of this research is based on the coupling of open EO and geospatial data and contemporary software and scientific processing and analysis techniques and methods. Given the proper attention and optimum use, this methodology has the potential to become an important operational tool against frost occurrence for researchers, planners, civil protection services and stakeholders in general.

In order to further develop the proposed methodology, it is necessary to study various areas with variations in the density and characteristics of their hydrographic network in relation to the frequency of frost. However, it must be noted, that if our methodology is applied in areas with different water bodies characteristics (volume, altitude etc.), it is expected to generate slightly different results (e.g., in areas close to Danube, where it would be the dominant water body, it would have the most important protective effect against frost). Thus, although the approach can be applied without bias in any site characterized by low temperatures and frost, the results must be carefully interpreted taking into account each time the peculiarities of each test site. Future research might focus on exploring the use of higher spatial resolution EO data than MODIS. Such analysis is expected to increase the spatial resolution of frost occurrence, emphasizing on the effect of rivers and lakes.

## 5. Conclusions

The main aim of this work was the investigation of the effect of water bodies on temperature fluctuations and the correlation patterns that existed between sea, lakes and rivers and frost frequency. The proposed methodology is based in the coupling of freely distributed EO and geospatial data, contemporary software and scientific processing and analysis techniques. The results showed in the

selected study area the existence of a protective buffer zone from frost at distances up to 20 km and 5 km from sea and water bodies, respectively. In the geographical scale of the study used in this research (of 1 km), sea proximity was proven to have the highest effect on frost fluctuations, followed by lake and river proximity. As for the influence of landscape characteristics on frost frequency, the most important factor was altitude, secondly slope whereas aspect and curvature did not show significant correlation. This was one of the primary applications in Europe which can lead to the planning of more targeted and effective mitigation measures against frost, through the more accurate quantification of frost effects.

**Author Contributions:** Conceptualization, P.L.; methodology, P.L., I.P. and N.S.; software, P.L., N.S. and K.K.; writing—original draft preparation, P.L., N.S., K.K., I.P. and G.P.P.; writing—review and editing, P.L., I.P., G.P.P., N.S. and K.K.; visualization, P.L., N.S. and K.K.; supervision, I.P. and G.P.P. All authors have read and agreed to the published version of the manuscript.

**Funding:** This research received no external funding.

**Conflicts of Interest:** The authors declare no conflict of interest.

## References

1. Kalogeropoulos, K.; Chalkias, C. Modelling the impacts of climate change on surface runoff in small Mediterranean catchments: Empirical evidence from Greece. *Water Environ. J.* **2013**, *27*, 505–513. [[CrossRef](#)]
2. Pulvirenti, L.; Pierdicca, N.; Chini, M.; Guerriero, L. An algorithm for operational flood mapping from Synthetic Aperture Radar (SAR) data using fuzzy logic. *Nat. Hazards Earth Syst. Sci.* **2011**, *11*, 529–540. [[CrossRef](#)]
3. Skakun, S.; Kussul, N.; Shelestov, A.; Kussul, O. Flood Hazard and Flood Risk Assessment Using a Time Series of Satellite Images: A Case Study in Namibia. *Risk Anal.* **2014**, *34*, 1521–1537. [[CrossRef](#)] [[PubMed](#)]
4. Stathopoulos, N.; Kalogeropoulos, K.; Polykretis, C.; Skrimizeas, P.; Louka, P.; Karymbalis, E.; Chalkias, C. Introducing Flood Susceptibility Index Using RS Data & GIS—Empirical Analysis in Sperchios River Basin, Greece. In *Remote Sensing of Hydro-Meteorological Hazards*, 1st ed.; Petropoulos, G.P., Islam, T., Eds.; CRC Press: Boca Raton, FL, USA, 2017; Volume 1, pp. 381–400. [[CrossRef](#)]
5. Stathopoulos, N.; Lykoudi, E.; Vasileiou, E.; Rozos, D.; Dimitrakopoulos, D. Erosion Vulnerability Assessment of Sperchios River Basin, in East Central Greece—A GIS Based Analysis. *Open J. Geol.* **2017**, *7*, 621–646. [[CrossRef](#)]
6. Stathopoulos, N.; Kalogeropoulos, K.; Dimitriou, E.; Skrimizeas, P.; Louka, P.; Papadias, V.; Chalkias, C. A Robust Remote Sensing–Spatial Modeling–Remote Sensing (RMR) Approach for Flood Hazard Assessment. In *Spatial Modeling in GIS and R for Earth and Environmental Sciences*, 1st ed.; Pourghasemi, H.R., Gokceoglu, C., Eds.; Elsevier: Amsterdam, The Netherlands, 2019; Volume 1, pp. 391–410. [[CrossRef](#)]
7. Fridley, J.D. Downscaling Climate over complex Terrain: High Finescale (<1.000 m) Spatial Variation of Near-Ground Temperatures in a Montane Forested Landscape (Great Smoky Mountains). *J. Appl. Meteorol. Clim.* **2009**, *48*, 1033–1049. [[CrossRef](#)]
8. Pouteau, R.; Rambal, S.; Ratte, J.P.; Goge, F.; Joffre, R.; Winkel, T. Downscaling MODIS-derived maps using GIS and boosted regression trees: The case of frost occurrence over the arid Andean highlands of Bolivia. *Remote Sens. Environ.* **2011**, *115*, 117–129. [[CrossRef](#)]
9. Daly, C.; Halbleib, M.; Smith, J.I.; Gibson, W.P.; Doggett, M.K.; Taylor, G.H.; Pasteris, P.P. Physiographically sensitive mapping of climatological temperature and precipitation across the conterminous United States. *Intern. J. Climatol. J. Roy. Meteor. Soc.* **2008**, *28*, 2031–2064. [[CrossRef](#)]
10. Holdaway, M. Spatial modeling and interpolation of monthly temperature using kriging. *Clim. Res.* **1996**, *6*, 215–225. [[CrossRef](#)]
11. Daly, C.; Gibson, W.P.; Taylor, G.H.; Johnson, G.L.; Pasteris, P. A knowledge-based approach to the statistical mapping of climate. *Clim. Res.* **2002**, *22*, 99–113. [[CrossRef](#)]
12. Vercauteren, N.; Destouni, G.; Dahlberg, C.J.; Hylander, K. Fine-resolved, near-coastal spatiotemporal variation of temperature in response to insolation. *J. Appl. Meteorol. Clim.* **2013**, *52*, 1208–1220. [[CrossRef](#)]
13. Ashcroft, M.B.; Chisholm, L.A.; French, K.O. The effect of exposure on landscape scale soil surface temperatures and species distribution models. *Landsc. Ecol.* **2008**, *23*, 211–225. [[CrossRef](#)]

14. Ashcroft, M.B.; Gollan, J.R. Fine—Resolution (25 m) topoclimatic grids of near—Surface (5 cm) extreme temperatures and humidities across various habitats in a large (200 × 300 km) and diverse region. *Int. J. Climatol.* **2012**, *32*, 2134–2148. [[CrossRef](#)]
15. Suggitt, A.J.; Gillingham, P.K.; Hill, J.K.; Huntley, B.; Kunin, W.E.; Roy, D.B.; Thomas, C.D. Habitat microclimates drive fine-scale variation in extreme temperatures. *Oikos* **2011**, *120*, 1–8. [[CrossRef](#)]
16. Francois, C.; Bosseno, R.; Vacher, J.J.; Segiun, B. Frost risk mapping derived from satellite and surface data over the Bolivian Altiplano. *Agric. For. Meteorol.* **1999**, *95*, 113–137. [[CrossRef](#)]
17. Blennow, K.; Persson, P. Modeling local-scale frost variations using mobile temperature measurements with GIS. *Agric. For. Meteorol.* **1998**, *89*, 59–71. [[CrossRef](#)]
18. Kerdiles, H.; Grondona, M.; Rodriguez, R.; Seguin, B. Frost mapping using NOAA AVHRR data in the Papean region, Argentina. *Agric. For. Meteorol.* **1996**, *79*, 157–182. [[CrossRef](#)]
19. Lindkvist, L.; Gustavsson, T.; Borgen, J. A frost assessment method for mountainous areas. *Agric. Forest Meteorol.* **2000**, *102*, 51–67. [[CrossRef](#)]
20. Rigby, J.R.; Porporato, A. Spring frost risk in a changing climate. *Geophys. Res. Lett.* **2008**, *35*. [[CrossRef](#)]
21. Cooper, W.C.; Young, R.H.; Turrell, F.M. Microclimate and physiology of citrus: Their relation to cold protection. *Agric. Sci. Rev.* **1964**, *2*, 38–50.
22. Hewitt, K. The idea of calamity in a technocratic age. In *Interpretations of Calamity from the Viewpoint of Human Ecology*, 1st ed.; Hewitt, K., Ed.; Allen & Unwin Inc.: Boston, MA, USA, 1983; Volume 1, pp. 3–32.
23. Stebelsky, I. Wheat yields and weather hazards in the Soviet Union. In *Interpretations of Calamity from the Viewpoint of Human Ecology*, 1st ed.; Hewitt, K., Ed.; Allen & Unwin Inc.: Boston, MA, USA, 1983; Volume 1, pp. 202–218. [[CrossRef](#)]
24. Martsole, J.D.; Gerber, J.F.; Chen, E.Y.; Jackson, J.L.; Rose, A.J. What do satellite and other data suggest about past and future Florida freezes. In Proceedings of the Annual Meeting of the Florida State Horticulture Society, Fresno, CA, USA, 18–21 November 1985; Volume 97, pp. 17–21.
25. Caprio, J.M.; Snyder, R.D. *Study to Improve Winterkill Parameters for a Winter Wheat Model. Task 1, a Study of the Relation between Soil Temperature at Three Centimeter Depth and Air Temperature*; Final Project Report. NASA Contract NAS9-16007; Plant and Soil Science Department, Montana State University: Bozeman, MT, USA, 1984; p. 76.
26. Cox, D.L.; Larsen, J.K.; Brun, L.J. Winter survival response of winter wheat: Tillage and cultivar selection 1. *Agron. J.* **1986**, *78*, 795–801. [[CrossRef](#)]
27. Condori, B.; Hijmans, R.J.; Ledent, J.F.; Quiroz, R. Managing Potato Biodiversity to Cope with Frost Risk in the High Andes: A Modeling Perspective. *PLoS ONE* **2014**, *9*, e81510. [[CrossRef](#)] [[PubMed](#)]
28. Snyder, R.L.; Melo-Abreu, J.D. *Frost Protection: Fundamentals, Practice and Economics*; Food and Agriculture Organization of the United Nations: Rome, Italy, 2005; Volume 1, pp. 1–240.
29. Larcher, W. *Ökophysiologie der Pflanzen 2001 Stuttgart*; Eugen Ulmer: Stuttgart, Germany, 2001; p. 302.
30. Eriksson, M. Winter road climate investigations using GIS. Doctoral Thesis, University of Gothenburg, Gothenburg, Sweden, 2001.
31. Shao, J.; Lister, P.J. The prediction of Road Surface State and Simulation of the Shading Effect. *Bound. Lay. Meteorol.* **1995**, *73*, 411–419. [[CrossRef](#)]
32. Louka, P.; Papanikolaou, I.; Petropoulos, G.P.; Stathopoulos, N. Temperature Fluctuation & Frost Risk Analysis on a Road Network, by Coupling Remote Sensing Data, Thermal Mapping and GIS Techniques. In *Remote Sensing of Hydro-Meteorological Hazards*, 1st ed.; Petropoulos, G.P., Islam, T., Eds.; CRC Press: Boca Raton, FL, USA, 2017; Volume 1, pp. 183–210. [[CrossRef](#)]
33. Chuanyan, Z.; Zhongren, N.; Guodong, C. Methods for modelling of temporal and spatial distribution of air temperature at landscape scale in the southern Qilian mountains, China. *Ecol. Model.* **2005**, *189*, 209–220. [[CrossRef](#)]
34. Tomlinson, C.J.; Chapman, L.; Thornes, J.E.; Baker, C. Remote sensing land surface temperature for meteorology and climatology: A review. *Meteorol. Appl.* **2011**, *18*, 296–306. [[CrossRef](#)]
35. Dubayah, R. Modeling a solar radiation topoclimatology for the Rio Grande River Basin. *J. Veg. Sci.* **1994**, *5*, 627–640. [[CrossRef](#)]
36. Dubayah, R.; Rich, P.M. Topographic solar radiation models for GIS. *Int. J. Geogr. Inf. Syst.* **1995**, *9*, 405–419. [[CrossRef](#)]

37. Safanda, J. Ground surface temperature as a function of slope angle and slope orientation and its effect on the subsurface temperature field. *Tectonophysics* **1999**, *306*, 367–375. [[CrossRef](#)]
38. Chapman, L.; Thornes, J.E.; Bradley, A.V. Modelling of road surface temperature from a geographical database. Part 2: Numerical. *Meteorol. Appl.* **2001**, *8*, 421–436. [[CrossRef](#)]
39. Jarvis, C.H.; Stuart, N. A comparison among strategies for interpolating maximum and minimum daily air temperatures. Part I: The selection of “guiding” topographic and land cover variables. *J. Appl. Meteorol.* **2001**, *40*, 1060–1074. [[CrossRef](#)]
40. Lookingbill, T.R.; Urban, D.L. Spatial estimation of air temperature differences for landscape-scale studies in montane environments. *Agric. For. Meteorol.* **2003**, *114*, 141–151. [[CrossRef](#)]
41. Chapman, L.; Thornes, J.E. Road Ice prediction using geomatics. *Sci. Total Environ.* **2006**, *360*, 1–3, 68–80. [[CrossRef](#)]
42. Bennie, J.; Kubin, E.; Wiltshire, A.; Huntley, B.; Baxter, R. Predicting spatial and temporal patterns of bud-burst and spring frost risk in north-west Europe: The implications of local adaptation to climate. *Glob. Chang. Biol.* **2010**, *16*, 1503–1514. [[CrossRef](#)]
43. Erlat, E.; Türkeş, M. Analysis of observed variability and trends in numbers of frost days in Turkey for the period 1950–2010. *Int. J. Climatol.* **2011**, *32*, 1889–1898. [[CrossRef](#)]
44. Stroppiana, D.; Antoninetti, M.; Brivio, P.A. Seasonality of MODIS LST over Southern Italy and correlation with land cover, topography and solar radiation. *Eur. J. Remote Sens.* **2014**, *47*, 133–152. [[CrossRef](#)]
45. Van de Kerchove, R.; Lhermitte, S.; Veraverbeke, S.; Goossens, R. Spatio-temporal variability in remotely sensed land surface temperature and its relationship with physiographic variables in the Russian Altay Mountains. *Int. J. Appl. Earth Obs.* **2013**, *20*, 4–19. [[CrossRef](#)]
46. Shao, J.C.; Swanson, R.; Patterson, P.; Lister, J.; McDonald, A.N. Variation of Winter Road Surface Temperature due to Topography and Application of Thermal Mapping. *Meteorol. Appl.* **1997**, *4*, 131–137. [[CrossRef](#)]
47. Radcliffe, J.E.; Lefever, K.R. Aspect influences on pasture microclimate at Coopers Creek, North Canterbury. *New Zeal. J. Agric. Res.* **1981**, *24*, 55–66. [[CrossRef](#)]
48. Oliver, W.W.; Dolph, K.L. Mixed-conifer seedling growth varies in response to overstory release. *For. Ecol. Manag.* **1992**, *48*, 179–183. [[CrossRef](#)]
49. Soderstrom, M.; Magnusson, B. Assessment of local agroclimatological conditions—A methodology. *Agric. For. Meteorol.* **1995**, *72*, 243–260. [[CrossRef](#)]
50. Oke, T.R. *Boundary Layer Climates*, 2nd ed.; Routledge: London, UK, 1987; p. 390. [[CrossRef](#)]
51. Daly, C.; Helmer, E.H.; Quinones, M. Mapping the climate of Puerto Rico, Vieques and Culebra. *Int. J. Climatol.* **2003**, *23*, 1359–1381. [[CrossRef](#)]
52. Gustavsson, T.; Borgen, J.; Eriksson, M. GIS as a tool for planning new road stretches in respect of climatological factors. *Theor. Appl. Climatol.* **1998**, *60*, 179–190. [[CrossRef](#)]
53. Dai, A.; Trenberth, K.E.; Karl, T.R. Effects of clouds, soil moisture, precipitation and water vapor on diurnal temperature range. *J. Climate* **1999**, *12*, 2451–2473. [[CrossRef](#)]
54. Geiger, R.F.; Aron, R.H.; Todhunter, P. *The Climate Near the Ground*, 6th ed.; Rowman & Littlefield Publishers Inc.: Lanham, MD, USA, 2003; p. 584. [[CrossRef](#)]
55. Stathopoulos, N.; Skrimizeas, P.; Kalogeropoulos, K.; Louka, P.; Tragaki, A. Statistical analysis and Spatial correlation of rainfall in Greece for a 20-year time period. In Proceedings of the 14th International Conference on Meteorology, Climatology and Atmospheric Physics, Alexandroupolis, Greece, 15–17 October 2018. EasyChair No. 737. [[CrossRef](#)]
56. Bouris, D.; Theodosiou, T.; Rados, K.; Makrogianni, M.; Koutsoukos, K.; Goulas, A. Thermographic measurement and numerical weather forecast along a highway road surface. *Meteorol. Appl.* **2010**, *484*, 474–484. [[CrossRef](#)]
57. MODIS Land-Surface Temperature Algorithm Theoretical Basis Document (LST ATBD) Version 3.3. Available online: [https://modis.gsfc.nasa.gov/data/atbd/atbd\\_mod11.pdf](https://modis.gsfc.nasa.gov/data/atbd/atbd_mod11.pdf) (accessed on 15 December 2019).
58. Chrysoulakis, N.; Abrams, M.; Feidas, H.; Velianitis, D. Analysis of ASTER multispectral stereo imagery to produce DEM and land cover databases for Greek islands: The REALDEMS project. In Proceedings of the e-Environment Progress and Challenge Conference, Vienna, Austria, 21–23 April 2004; pp. 411–424.
59. Miliareisis, G.C.; Paraschou, C.V. An evaluation of the accuracy of the ASTER GDEM and the role of stack number: A case study of Nisiros Island, Greece. *Remote Sens. Lett.* **2011**, *2*, 127–135. [[CrossRef](#)]

60. GeoDa Center, Center for Spatial Data Science. University of Chicago: Chicago, IL, USA. Available online: <http://geodacenter.github.io/> (accessed on 10 August 2019).
61. Louka, P.; Papanikolaou, I.; Petropoulos, G.P.; Stathopoulos, N. A Deterministic Model to Predict Frost Hazard in Agricultural Land Utilizing Remotely Sensed Imagery and GIS. In *Geospatial Technology for Water Resource Development*, 1st ed.; Srivastava, P.K., Pandey, P.C., Kumar, P., Raghubanshi, A.S., Han, D., Eds.; Taylor and Francis: Abingdon, UK, 2015; pp. 213–241.
62. Koenig, W.D. Spatial autocorrelation of ecological phenomena. *Trends Ecol. Evol.* **1999**, *14*, 22–26. [[CrossRef](#)]
63. Anselin, L.; Syabri, I.; Kho, Y. GeoDa: An introduction to spatial data analysis. *Geogr. Anal.* **2006**, *38*, 5–22. [[CrossRef](#)]
64. Jenks, G.F. The data model concept in statistical mapping. *Int. Yearb. Cartogr.* **1967**, *7*, 186–190.



© 2020 by the authors. Licensee MDPI, Basel, Switzerland. This article is an open access article distributed under the terms and conditions of the Creative Commons Attribution (CC BY) license (<http://creativecommons.org/licenses/by/4.0/>).